RSC Advances

PAPER

View Article Online
View Journal | View Issue

Cite this: *RSC Adv.*, 2023, **13**, 20984

Nickel nanoparticle decorated silicon carbide as a thermal filler in thermal conductive aramid nanofiber-based composite films for heat dissipation applications

Xin Wang,[ab] Huarui Dong,[ab] Qingyi Ma,[ac] Yanjie Chen,[ab] Xueling Zhao[ab] and Lifei Chen *[ab]

Aramid nanofibers (ANFs) have shown potential applications in the fields of nanocomposite reinforcement, battery separators, thermal insulation and flexible electronics. However, the inherent low thermal conductivity limits the application of ANFs, currently, to ensure long lifetime in electronics. In this work, new nickel (Ni) nanoparticles were employed to decorate the silicon carbide (SiC) filler by a rapid and non-polluting method, in which nickel acetate tetrahydrate ($Ni(CH_3COO)_2 \cdot 4H_2O$) and SiC were mixed and heated under an inert atmosphere. The composites as thermal fillers were applied to prepare an aramid nanofiber (ANF)-based composite film. Our results showed that the decoration of SiC by an appropriate amount of Ni nanoparticles played an important role in improving the thermal conductivity, hydrophobicity, thermal stability, and puncture resistance of the ANF composite film. After adjusting the balling time at 10 h, the optimized content of 10 mol% Ni nanoparticles improved the thermal conductivity to 0.502 W m^{-1} K^{-1}, 298.4% higher than that of the original ANF film. Moreover, increasing the content of thermal fillers to 30 wt% realized a high thermal conductivity of 0.937 W m^{-1} K^{-1}, which is 643.7% higher than that of the pristine ANF film. Moreover, the compatibility between thermal fillers and ANFs and thermal stability were improved for the ANF-composite films. The effective heat transfer function of our composite films was further confirmed using a LED lamp and thermoelectric device. In addition, the obtained composite films show certain mechanical properties and better hydrophobicity; these results exhibit their great potential applications in electronic devices.

Received 19th May 2023
Accepted 23rd June 2023

DOI: 10.1039/d3ra03336h

rsc.li/rsc-advances

Introduction

Polymer fiber thermal conductive films are an emerging material for thermal management with excellent properties such as lightweight, flexibility and electrical insulation in the fields of nanocomposite reinforcement, high-performance heating systems and flexible electronics.[1–3] In particular, electronic devices are in great need of paper-based films with anisotropic thermal conductivity and good mechanical properties.[4] Poly(*p*-phenylene terephthalate) (PPTA) fibers, known as aramid fibers, have rigid molecular chains that are partially connected and extended. The molecular chains interact with each other through a strong and highly oriented network of hydrogen bonds. Aramid fibers have excellent mechanical properties, outstanding thermal stability, high chemical resistance and flame retardancy, which are considered one of the best candidates among most polymers for the preparation of thermal conductive films.[5–8] However, the structure and size difference between macroscopic aramid fibers and fillers make them unsuitable for the preparation of flexible thermal conductive films. Macroscopic aramid fibers also have disadvantages such as smooth intrinsic surface, few active functional groups, and chemical inertness. This may cause poor interfacial bonding, which is unfavourable for the preparation of flexible composite thermal conductive films. In contrast, aramid nanofibers, with high tensile strength and low dielectric properties, have nanoscale size, large aspect ratio and high specific surface area while maintaining the original excellent properties of macroscopic fibers.[9] However, the low thermal conductivity of ANFs severely limits their further application in the electronic and electrical fields. As far as we know, the thermal conductivities of ANF-based composites have not been widely investigated, and it is still urgent to develop novel aramid nanofiber (ANF)-based thermal conductive composites, improving the thermal

[a]*School of Energy and Materials, Shanghai Key Laboratory of Engineering Materials Application and Evaluation, Shanghai Polytechnic University, Shanghai 201209, China. E-mail: lfchen@sspu.edu.cn*

[b]*Shanghai Thermophysical Properties Big Data Professional Technical Service Platform, Shanghai Engineering Research Center of Advanced Thermal Functional Materials, Shanghai 201209, China*

[c]*School of Resources and Environmental Engineering, Shanghai Polytechnic University, Shanghai 201209, P. R. China*

conductivities, thermal stability and their heat dissipation performance to meet the device life.

Generally, it is an effective approach to introduce highly thermally conductive fillers including carbon-based fillers, metal fillers and ceramic fillers into a polymer composite. Among them, silicon carbide (SiC) has irreplaceable application advantages in the fields of high temperature, high frequency, high power devices and aerospace.[10–12] As a ceramic filler, silicon carbide has the characteristics of high thermal conductivity, high temperature stability, low conductivity, high strength and chemical corrosion resistance. Another advantage of SiC is super hydrophobicity, which will greatly affect the reliability and lifetime of electronic devices.[13,14] However, the dispersion of ceramic fillers in polymeric substrates remains a problem.[15,16] If the addition amount of thermal fillers is too high, the thermal resistance at the filler–substrate interface will increase dramatically, which adversely affects its thermal conduction.[17,18] Previous reports have demonstrated that many physical and electrical properties of semiconductor materials, such as the photocatalytic, magnetic, and dielectric properties, can be enhanced by introducing foreign metallic ions.[19–22] In this case, a small amount of metal filler addition is suitable for improving the thermal conductivity while maintaining the insulating properties of the material.[23–26]

Currently, metal nanoparticle attachment on the surfaces of ceramic fillers has been performed successfully, in which the metal-decorated hybrid fillers exhibit lower porosity, better dispersion and good interfacial contact. The synergistic effect of ceramic and metal fillers on the surface, therefore, enhances the thermal conductivities of composites.[25,27] Several studies have reported the improved heat dissipation behaviour of polymer composite materials in electronic equipment.[27–31] For the preparation process, the 'mix and heat' method to produce many thermal conductive fillers decorated with metal nanoparticles without any reducing agent is rapid, simple, and non-polluting.[32] This method can be extended to deposit other metals or metal oxides on different substrate surfaces. For example, Sagar Kumar Nayak *et al.* prepared alumina-based composite thermal fillers decorated by silver nanoparticles (Ag/α-Al_2O_3) using this method.[33] The related thermal conductivity of epoxy composites was improved by 9.8 times when compared to the epoxy resin. However, preparation and performance studies of thermal conductive films with metal-decorated ceramic fillers are necessary but rarely reported nowadays.

Nickel (Ni) is a metal element with good thermal conductivity, mechanical properties, and chemical stability as well as an excellent electromagnetic shielding role.[34] As previously reported, good electromagnetic properties can be obtained for composites by introducing kinds of metal nanoparticles (such as Sn, Co, Ce, and Ag).[35–38] Therefore, Ni nanoparticle-deposited SiC (Ni/SiC) is expected to improve both thermal conductivity and electromagnetic shielding absorption of polymer fiber thermal conductive films.[39,40] For example, Bin Yang *et al.*[41] proposed the use of proton donor-assisted deprotonation to prepare ANFs in a time-saving and efficient manner. The prepared ANF films not only exhibit a small diameter but also ultra-high strength and toughness.

In this study, novel Ni-decorated thermal fillers (Ni/SiC) were prepared by a 'mix and heat' method to fabricate aramid nanofiber-based thermal conductive composites. The composite fillers with a small size and good surface loading were obtained by optimizing the ball milling time to 10 h. The effect of Ni loading content and the filling amount of Ni/SiC fillers (30 wt%) on the performance of the ANF-based thermal conductive films was studied. As a result, a high thermal conductivity of 0.937 W m^{-1} K^{-1} for ANF-composites was achieved, 643.7% higher than that of the pristine ANF film (0.126 W m^{-1} K^{-1}). Meanwhile, the hydrophobicity and thermal stability of the ANF-composites were enhanced, together with a good tensile strength (~68.12 Mpa at 30 wt%). Furthermore, the composites were applied on a LED device and thermoelectric device successfully, showing excellent heat dissipation capacity, exhibiting great potential for application in flexible electronic devices.

Experimental section

Materials

Silicon carbide (SiC, Adamas), nickel acetate tetrahydrate ($Ni(CH_3COO)_2 \cdot 4H_2O$, 99.9%, AR, Adamas), potassium hydroxide (≥95.0%, Flakes, Reagent) and dimethyl sulfoxide (DMSO, 99.9%, ACS, Adamas) were purchased from Tansoole. Aramid fibers (Kevlar) were purchased from Dupont Company. Deionized (DI) water was used in the experiments.

Preparation of the SiC-composite decorated by Ni nanoparticles

A certain amount of SiC and $Ni(CH_3COO)_2 \cdot 4H_2O$ was fully mixed by ball milling and then heated at high temperature in a tube furnace. The ball milling process was conducted with a planetary ball milling machine at 400 rpm with zirconia balls. The final heating temperature was set to 500 °C and the mixture was kept heating for 2 h. By adjusting the ball milling time (0 h, 5 h, and 10 h), the Ni/SiC composites with 5 mol% Ni nanoparticles (*i.e.*, 5 mol% Ni/SiC-0, 5 mol% Ni/SiC-5, 5 mol% Ni/SiC-10) were prepared. The composite thermal conductive fillers with good loading of Ni were selected. By varying the amount of $Ni(CH_3COO)_2 \cdot 4H_2O$, the Ni/SiC composite with different Ni contents was obtained and the samples were denoted as 5 mol% Ni/SiC, 10 mol% Ni/SiC, and 20 mol% Ni/SiC, respectively.

Fabrication of aramid nanofiber-based thermal conductive films

Fig. 1 shows the preparation of ANF composite films with Ni/SiC as thermal fillers. Firstly, 0.6 g of aramid fiber and 0.9 g of KOH were added to 300 ml of DMSO. Deionized water was added to the mixture according to the volume ratio of H_2O : DMSO (1 : 25). The solution was stirred at 800 rpm for 36 h at room temperature (25 °C) to obtain a uniform and dark red ANF/DMSO/H_2O solution. And then 600 ml of H_2O was injected into the dark red solution. The mixed solution was stirred continuously with a magnetic stirrer for 1 h to form the colloidal ANF,

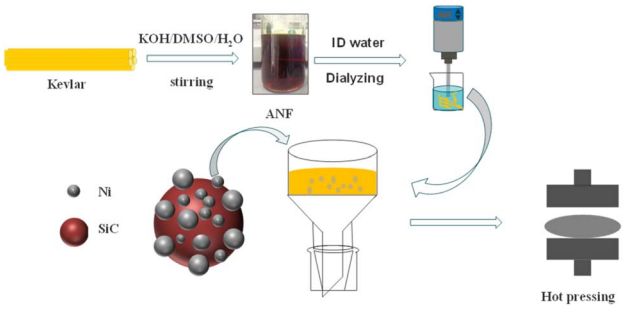

Fig. 1 Preparation of ANF composite films with Ni/SiC as thermal fillers.

which was further separated by vacuum filtration using a Buchner funnel. To completely remove the residual KOH and DMSO, the ANF was repeatedly washed with H_2O until the filtrate was neutral. After that, 0.2 g of the colloidal ANF was dispersed in 400 ml of H_2O for one hour. A homogeneous ANF/H_2O suspension with a concentration of 0.5 mg ml^{-1} was obtained. The suspension was stirred vigorously using a high-speed homogenizer for 5 min at 20 000 rpm and then stirred using a magnetic stirrer for 1 h at 500 rpm. The stable ANF dispersion was then prepared. The dispersion was continuously vacuum-filtrated with a 0.2 μm-pore PTFE membrane for approximately 3 h to obtain a wet ANF membrane. Finally, the dispersion was further dried at 100 °C for 20 min to obtain the pure ANF film.

The preparation process of the composite thermal conductive film is the same as that of the pure ANF film. The thermal conductive fillers with different Ni contents were placed in the dispersion, respectively. The dispersion was stirred for 2 h after ultrasonic treatment for 10 min, followed by vacuum-assisted filtration. The composite films were then dried at 100 °C for 20 min. The obtained ANF-based thermal conductive films with different Ni contents were recorded as ANF + SiC, ANF + 5 mol% Ni/SiC, ANF + 10 mol% Ni/SiC, and ANF + 20 mol% Ni/SiC, respectively. For selecting better thermal conductivity, the weight fraction of thermal conductive fillers was changed, and ANF-based composite thermal conductive films containing 0, 10, 20, and 30 wt% thermal fillers were also prepared.

Characterization

A scanning electron microscope (SEM) was used to characterize the morphology of the thermal fillers and thermal conductive films. The surface element distribution of the fillers was analyzed using an energy dispersive spectrometer (EDS). The phase composition and crystal structure of the fillers were analyzed by X-ray diffraction (XRD).

The thermal conductivity (K, W m^{-1} K^{-1}) of the aramid fiber-based composite films was measured using a C-Therm TCI thermal conductivity meter. The film used in thermal conductivity detection was a circular film with a diameter of 4 cm and a thickness of about 0.261 ± 0.05 mm. For each sample, we tested three films and the average thermal conductivity was recorded.

The TGA-DTA (Germany Trisch Company) measurement was performed to study the thermal stability of the thermal composite film. The temperature for the composites in nitrogen was increased to 700 °C gradually with a heating rate at 10 °C min^{-1}. The tensile strength of films was tested using an auto tensile tester. It is necessary to cut the samples into long strips, while ensuring that the edges of the cut samples are smooth and nano-defective. The actual width, thickness and distance of the sample are then measured. A Vernier caliper was used to measure the width and standard distance of each sample, and a thickness meter was used to measure the thickness. The width and thickness were recorded at three points within the standard distance, and the average value was obtained. The speed for the tensile test was 10 mm min^{-1}. The tensile test was performed according to GB/T10004-2008 experimental standard.

Results and discussion

Characterization and analysis of Ni/SiC composite thermal fillers

Fig. 2 shows the surface morphology and the distribution of Ni element on the surface of 5 mol% Ni/SiC at different ball milling times. When the ball milling time increased from 0 h to 10 h, the acetate salt and silicon carbide were fully mixed, the average size of Ni nanoparticles decreased and Ni nanoparticles were more uniformly distributed on the surface of silicon carbide (Fig. 2b and c). Meanwhile, increasing the ball milling time decreased the average particle size of silicon carbide (as shown in Fig. 3) and increased the surface area of silicon carbide. This is because the ball milling may increase the active sites on the surface of the thermal fillers. In this case, the SiC particles collide with each other during the ball milling process, causing wear to the SiC structure, and thereby the reduced average particle size of the silicon carbide. The elemental content of Ni nanoparticles on the 5 mol% Ni/SiC surface after 10 h of ball milling was significantly increased as seen in the elemental distribution in Fig. 2c1.

The XRD patterns of the pure SiC and Ni-decorated SiC are shown in Fig. 4. Fig. 4a shows the powder XRD pattern of the undecorated SiC sample, together with its Rietveld refinement (weighted profile factor, R_{wp} = 13%). The peaks could be well indexed to the hexagonal structure (wurtzite-type, space group $P6_3mc$), the lattice parameters of a = 3.081 Å and c = 15.115 Å

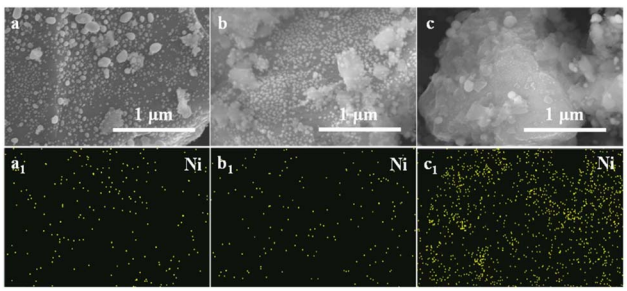

Fig. 2 SEM images (a–c) and EDS maps (a1–c1) of 5 mol% Ni/SiC fillers prepared by 0 h, 5 h and 10 h of ball milling, respectively.

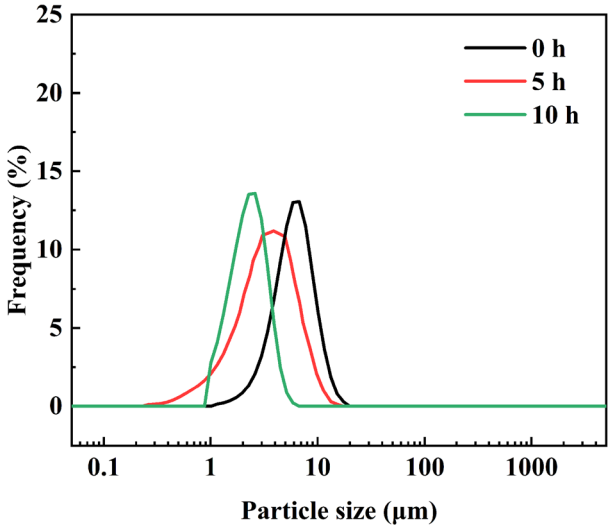

Fig. 3 Particle size distribution of composite thermal fillers prepared after different ball milling times.

were obtained, and the unit cell volume was $V = 120$ Å3. The strongest intensity of the (111) diffraction peak is found at around 36.8° and corresponds to its polycrystalline structure. Fig. 4b shows the signature spectrum of nickel around 44.591° and 51.946°, corresponding to the (111) and (200) crystal planes of Ni (the location indicated by the black dotted lines), respectively.

Compared to the diffraction spectra of pristine SiC, the diffraction peak intensity at 36.8° of 5 mol% Ni/SiC-0 corresponding to the (111) crystal plane of SiC (the location indicated by the orange dotted lines in Fig. 4a) was decreased, which is due to the deposition of Ni nanoparticles. In the spectra of 5 mol% Ni/SiC-5, the characteristic diffraction peaks of the same crystalline plane increased obviously. It can be speculated that the acetate salt played a protective role and a small amount of impurities was removed from the surface of silicon carbide during the ball milling process. The particles' collision may contribute to the increase of (111) crystal planes and the decrease of other crystal planes. The smaller size of Ni nanoparticles also improves the characteristic diffraction peaks of SiC crystal planes obviously. When the ball milling time was increased to 10 h, the diffraction peak of the (111) crystal surface of SiC decreased again. This is due to the longer ball milling time that may have a certain wear on the structure of silicon carbide and weaken the diffraction peak of SiC, and consequently, the interaction of SiC molecules was weakened, causing a decreased diffraction peak of SiC.

Based on the higher loading content and uniform distribution of Ni nanoparticles at 10 h of ball milling, the composite thermal fillers with different contents of Ni nanoparticles (5 mol% Ni/SiC-10, 10 mol% Ni/SiC-10, and 20 mol% Ni/SiC-10) were then prepared and their structures were then characterized by XRD (Fig. 4b). It was found that a new characteristic diffraction peak of Ni nanoparticles appeared at 76.465°, corresponding to the (220) crystal planes of Ni. The diffraction peak

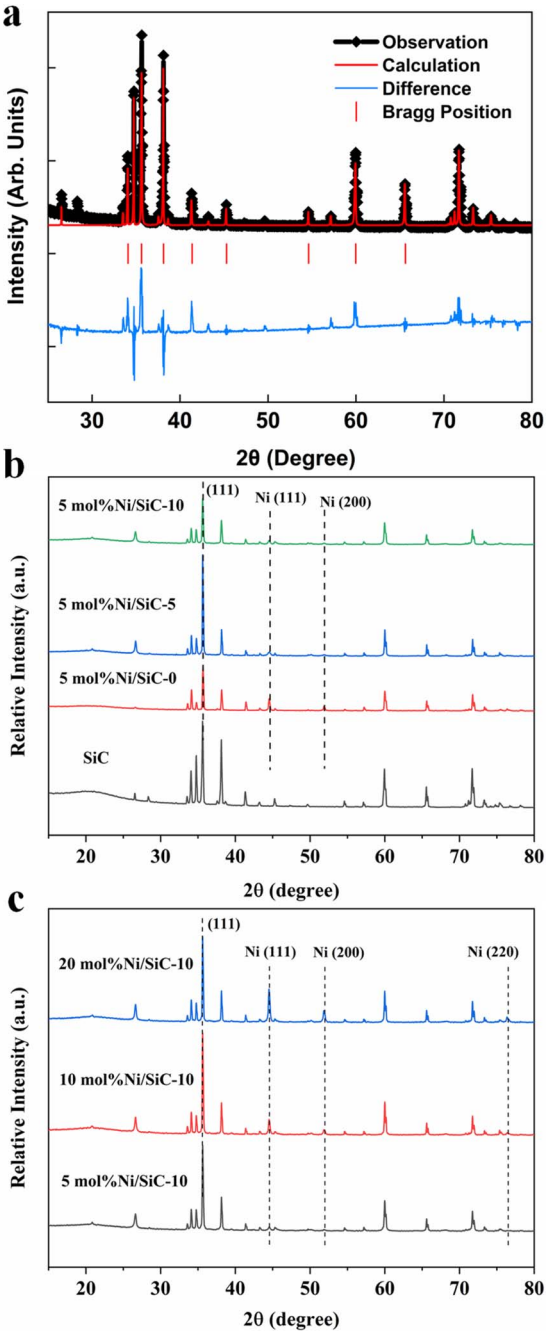

Fig. 4 (a) XRD pattern of SiC with its Rietveld refinement; (b) XRD patterns of SiC and 5 mol% Ni/SiC fillers prepared at different times; (c) XRD patterns for composite thermal fillers with different metal nanoparticle contents.

intensity increased with the increase of Ni nanoparticle deposition (marked by a black dashed line), indicating the better crystallinity of Ni nanoparticles. The smaller half-peak value (calculated using Jade software) indicated the increase of average particle size and loading content of Ni nanoparticles. The diffraction peak of the (111) crystal plane of SiC also increased. This may be due to the increase of Ni nanoparticle content to avoid the damage to the SiC crystal surface during

ball milling. Fig. 5 shows the surface morphology of the composite thermal fillers with different contents of Ni nanoparticles. The larger average size of Ni nanoparticles on the surface can be clearly seen, which is probably due to the secondary nucleation of small-sized Ni particles with more amount of Ni nanoparticle addition.[42] However, when Ni deposition exceeded a certain amount, the adjacent nanoparticles easily gathered together, leading to a larger particle size. Fig. 5c clearly shows the nanoparticle agglomeration on the surface of the sample 20 mol% Ni/SiC-10. By the way, the uneven distribution of metal nanoparticles on the surface is another factor for this particle aggregation.

XRD characterization and analysis of ANF-based thermal conductive films

XRD was used to analyze the phase composition and structure of ANF-based thermal conductive films under different Ni contents. As shown in Fig. 6, two broad and small peaks at $2\theta = 20.8°$ and 23.1° appear in the XRD spectrum for the pure ANF film, which correspond to the (110) and (220) crystal planes of ANFs, respectively. It is well known that aramid fibers contain ordered and densely arranged hydrogen bonds, and thereby have high crystallinity. During the splitting of aramid fibers, the ordered structure was disrupted, so no sharp peaks appear in the XRD spectra of the pure ANF film. The appearance of crystal planes of SiC and Ni nanoparticles suggested the successful dispersion of SiC-based composite thermal fillers in the ANF substrate. In contrast, with the addition of thermal fillers, the characteristic diffraction peaks of ANFs become broadened and weaker, indicating a perturbed orientation structure of ANFs.

Analysis of thermal conductivity of ANF-based thermal conductive films

The thermal conductivity of the pure ANF film and ANF-based films with different Ni nanoparticles was tested using a thermal conductivity meter. As shown in Fig. 7, the thermal conductivity of the pure ANF film (0.126 W m^{-1} K^{-1}) is relatively low. This is due to the weak chain bonds and multiple phonon scattering, which are caused by chain distortion, entanglement and external defects. The incorporation of SiC and Ni nanoparticles significantly increased the thermal conductivity to 0.35 W m^{-1} K^{-1} for the 5 mol% Ni/SiC–ANF composite film, which is 177% higher than that of the pure ANF film. This can be explained by the improved contact between the fillers and ANFs when metal Ni nanoparticles were deposited on the surface of SiC. In this case, the metal nanoparticles became the

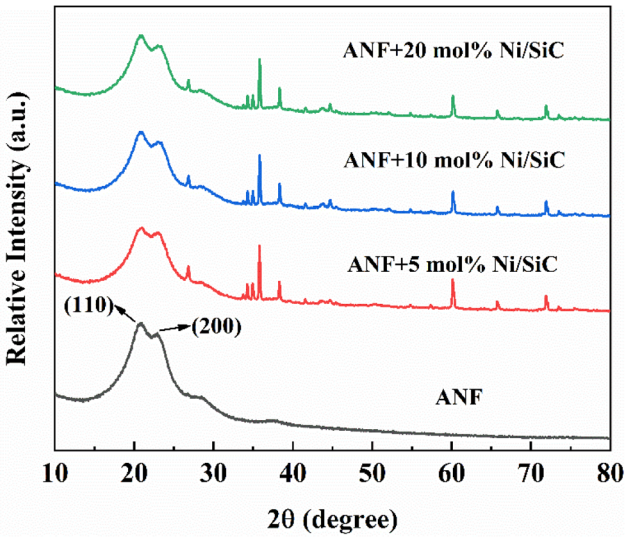

Fig. 6 XRD patterns of the pure ANF film and ANF-based composite thermal conductive film.

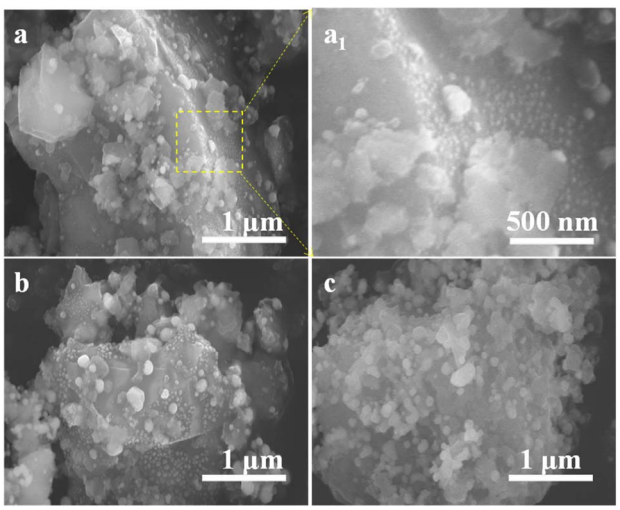

Fig. 5 SEM images of (a) 5 mol% Ni/SiC, (b) 10 mol% Ni/SiC, and (c) 20 mol% Ni/SiC; (a1) is the magnified SEM image of the part marked in (a).

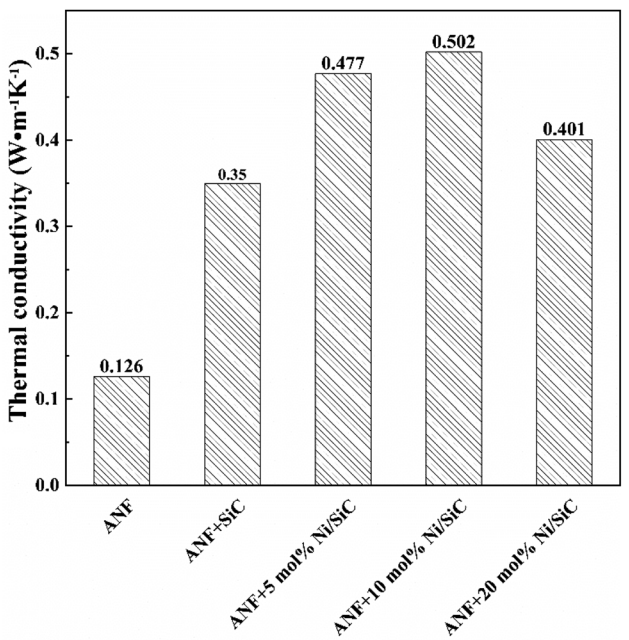

Fig. 7 Thermal conductivity of ANF-based thermal conductive films under the condition of different loading and the pure ANF film.

bridge for phonon transfer and phonon scattering was attenuated, providing an effective thermal conductivity pathway. Moreover, unlike general polymers, the fibers do not completely wrap thermal conductive fillers, enabling effective contact at low content and thereby the improvement of the thermal conductivity. When the loading of Ni nanoparticles increased from 5 mol% to 10 mol%, the increased Ni particle size further enlarges the contact area and reduces the interfacial thermal resistance, promoting the phonon transfer between thermal fillers and the ANF substrate. As a result, the thermal conductivity of 10 mol% Ni/SiC reaches 0.502 W m^{-1} K^{-1}, 298% higher than that of the pure ANF film and 43% higher than that of the SiC-based ANF film. Continuously increasing the Ni nanoparticle load to 20 mol% does not further enhance the thermal conductivity; the thermal conductivity of 20 mol% Ni/SiC is 0.401 W m^{-1} K^{-1}. This is because agglomeration of Ni nanoparticles on the surface limited the conduction and dispersion of thermal fillers in the ANF substrate, causing a high interfacial thermal resistance.

SEM characterization and analysis of ANF-based thermal conductive films

To further study the effect of composite fillers on the thermal conductive films, the ANF-based composite films with different weight fractions of Ni-decorated SiC thermal filler (from 10 to 30 wt%) were prepared. They were denoted as 10 mol% Ni/SiC10 wt%–ANF, 10 mol% Ni/SiC20 wt%–ANF, and 10 mol% Ni/SiC30 wt%–ANF, respectively. As shown in Fig. 8, the surface of the ANF-based thermal conductive film becomes rougher and rougher while increasing the weight fraction of thermal fillers gradually. The ANFs tend to be arranged in a shoulder-to-shoulder pattern in local regions; this is probably due to the multiple hydrogen bonding interaction of ANFs.

Effect of amount of thermal fillers on the performance of ANF-based composite films

Fig. 9 shows the effect of weight fraction of thermal fillers on the thermal conductivity of ANF-based composite films. With the increase of composite thermal fillers, the thermal conductivity of the composite films was gradually enhanced. This can be attributed to a more effective thermal conductive network with more mutual contact and lower interfacial thermal resistance. When the filling amount of fillers reached 30 wt%, the thermal conductivity of the composite film reached 0.937 W m^{-1} K^{-1}, which is ~643.7% higher than that of the pure ANF film.

To evaluate the heat dissipation effect of the composite films, the measurement of temperature on a LED lamp (3 W) was performed using different composite thermal conductive films at ambient temperature of 25 °C. Generally, the lifetime of a LED lamp is related to the operating temperature and high temperature has an adverse effect on its reliability. As shown in Fig. 10a, the LED lamp was placed flat on the surface of the thermally conductive film and connected to a power supply. The temperature on the top of the LED lamp was recorded with a thermocouple. We repeated the measurement three times and took an average temperature for each sample in the test. In Fig. 10b, it was found that the surface temperatures of the four kinds of films increased with the increment in the heating time. Specifically, the lowest surface temperature is observed in 10 mol% Ni/SiC30 wt%–ANF (~33 °C), followed by 20 mol% Ni/SiC30 wt%–ANF (~35 °C), 10 mol% Ni/SiC30 wt%–ANF (~38 °C) and finally pure ANF (~39.5 °C). These results indicated the heat dissipation capacity of the composite films. Expectedly, the surface temperature of the LED lamp with 10 mol% Ni/SiC30 wt%–ANF was the lowest in comparison to other films, which is in agreement with the thermal conductivity of these composite films.

To further confirm the effective heat transfer for our composite films, a thermoelectric device was introduced as shown in Fig. 10c. The heat storage materials (paraffin) were installed in the box wrapped with heat insulation materials. When the paraffin was heated to 100 °C and transformed into a liquid state, the box filled with paraffin was placed on the thermal conductive film immediately, and the output voltage for the device was recorded using a multimeter. Before heating,

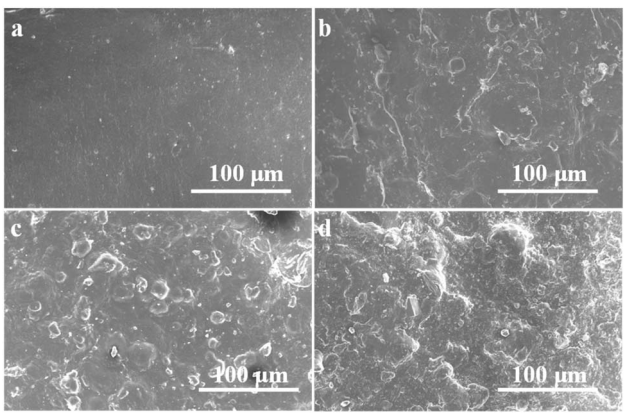

Fig. 8 SEM images of (a) ANFs, (b) 10 mol% Ni/SiC10 wt%–ANF, (c) 10 mol% Ni/SiC20 wt%–ANF, and (d) 10 mol% Ni/SiC30 wt%–ANF thermal conductive films.

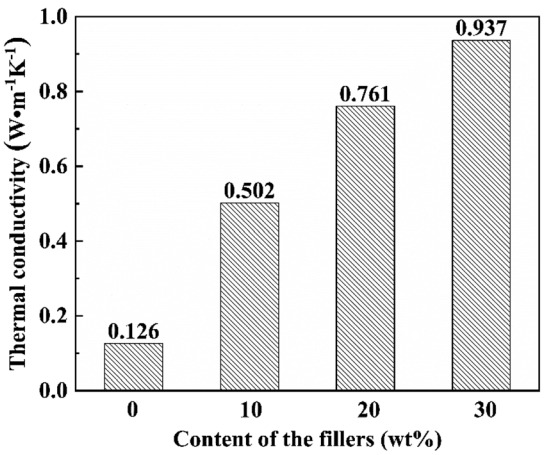

Fig. 9 Thermal conductivity of ANF-based thermal conductive films with different composite filler contents.

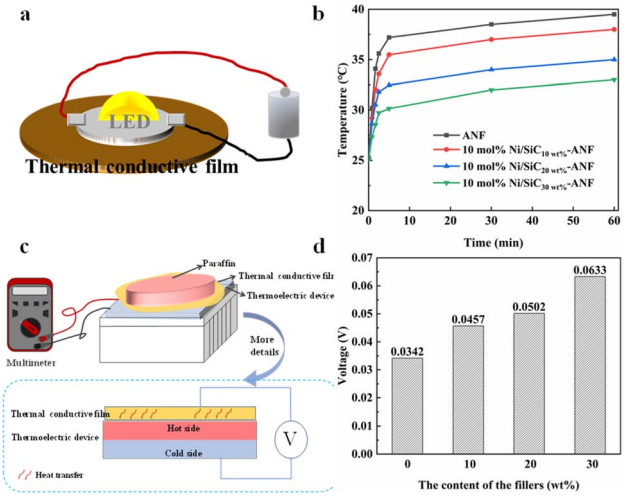

Fig. 10 (a) Schematic of the LED device test setup using the ANF-based thermal conductive film as the substrate; (b) results obtained using the setup (a); (c) schematic of heat transfer application on a thermoelectric device of composite films; (d) voltages obtained using the setup.

the paraffin is ensured in a solid state completely at room temperature (25 °C) every time. As can be seen from Fig. 10d, the trend of the output voltage is in line with the thermal conductivity change for ANF-based composite films. This result suggested that ANF-based composite films can also be used as the thermal interface material to effectively transfer heat according to our requirement.

The contact angle (CA) test is usually used to characterize the hydrophilicity and hydrophobicity of a material's surface. When the contact angle is greater than 90°, the material appears hydrophobic. Fig. 11 presents the images of water droplets falling on the surfaces of different composite thermal conductive films. The contact angles for ANF-based films doped with 0, 10, 20, and 30 wt% thermal fillers were 90.5°, 107.5°, 109.5°, and 113°, respectively. The enlarged contact angle means a better hydrophobicity and waterproof property for the Ni/SiC-based composite film than the pure ANF film, which helps to prolong the real lifetime of a thermal-electronic device.

The thermal stability of a material plays an important role in determining its operating temperature. The thermogravimetric analysis (TGA) curves of the ANF-based thermal conductive film are shown in Fig. 12a. The TGA results showed that the initial thermal decomposition temperature for the pristine ANF film, 10 mol% Ni/SiC10 wt%–ANF, 10 mol% Ni/SiC20 wt%–ANF and 10 mol% Ni/SiC30 wt%–ANF are 490 °C, 506 °C, 506 °C and 525 °C, respectively. The higher decomposition temperature of the composite thermal films proved that thermal filler addition can enhance the thermal stability. Moreover, under the same weight loss rate condition, increasing weight content of thermal fillers can further prevent thermal decomposition of ANF-based composite films. By the way, due to the excellent thermal stability of SiC, the residue yields were proportional to the mass fraction of SiC in the ANF-based thermal conductive films in our test.

Stress and strain are important parameters to evaluate the mechanical properties of a composite material. Fig. 12b shows the stress–strain curves of the pure ANF film and ANF-based composite thermal conductive films. The tensile strengths of the thermal conductive films with different filler contents (0, 10, 20, and 30 wt%) were 111.94, 98.6, 79.35, 75, and 68.12 Mpa, respectively. The standard deviations of the tensile strengths were 1.23, 1.04, 1.01, 0.51, and 0.42 Mpa. Benefiting from the high aspect ratio of ANFs and ANF chains and their interconnection with multiple hydrogen bonding, it can be found that the pure ANF film exhibited excellent mechanical strength and toughness. While increasing the composite fillers, the tensile strength of the composite films was weakened. This can be explained by the separation of composite fillers partially and reduction of the contact in ANF chains, which thereby decreased the hydrogen bonding density. Among all samples, the tensile strength of 10 mol% Ni/SiC30 wt%–ANF was reduced by 39.1% compared to the pure ANF film. However, all samples still show good mechanical properties with stresses around 60–120 Mpa and strain values above 50%.[43]

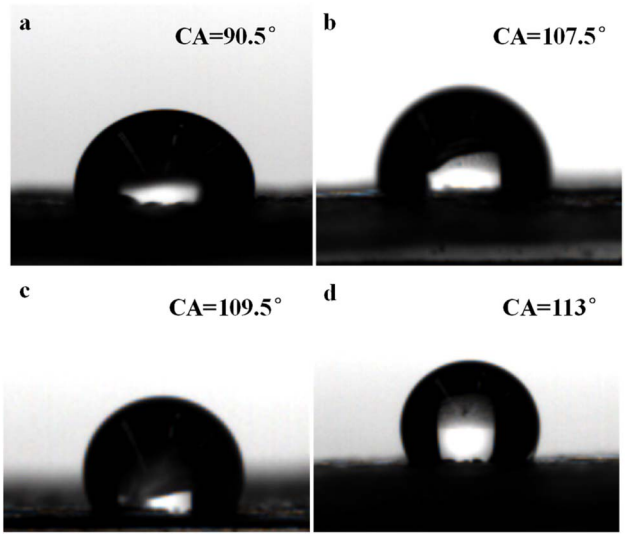

Fig. 11 Contact angle images of (a) ANF, (b) 10 mol% Ni/SiC10 wt%–ANF, (c) 10 mol% Ni/SiC20 wt%–ANF, and (d) 10 mol% Ni/SiC30 wt%–ANF thermal conductive films.

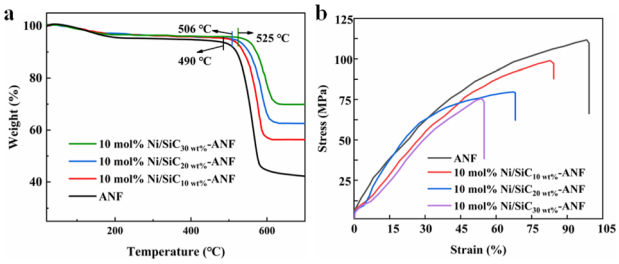

Fig. 12 (a) TGA and (b) tensile strength of ANF films and ANF-based composite thermal conductive films with different composite filler contents.

Conclusions

In this work, a Ni nanoparticle decorated SiC composite was prepared by using a rapid and non-polluting method, in which nickel acetate tetrahydrate and silicon carbide were mixed and heated to the decomposition temperature. When employing the Ni/SiC composite as a thermal filler, the synergistic effect of Ni nanoparticles and SiC improved the thermal conductivity, thermal stability, and puncture resistance of ANF-based composite films.

(1) Adjusting the ball milling time at 10 h, the thermal conductivity (0.502 W m^{-1} K^{-1}) of the ANF composite film with 10 mol% Ni/SiC was increased by 298.4% in comparison to the pure ANF film (0.126 W m^{-1} K^{-1}).

(2) When the filling amount of the thermal fillers was optimized, the thermal conductivity of 10 mol% Ni/SiC30 wt%–ANF was improved to 0.937 W m^{-1} K^{-1}, 643.7% higher than that of the pure ANF film. The composite film can be used as a thermal interfacial material to transfer heat quickly from the energy store to the heat-needed side.

(3) The decomposition temperature and the final residual mass of 10 mol% Ni/SiC30 wt%–ANF were the highest one among those of other composite films, indicating its good thermal stability. With the increase of thermal fillers, the hydrophobicity of the composite thermal film was enhanced, and the tensile strength decreased slightly but it still maintained certain mechanical properties.

Author contributions

Xin Wang: investigation, writing – review & editing, funding acquisition. Huarui Dong: data curation, formal analysis, writing – original draft. Qingyi Ma: data curation, formal analysis. Yanjie Chen: data curation, formal analysis. Xueling Zhao: writing – review & editing, funding acquisition. Lifei Chen: supervision, writing-review & editing, project administration.

Conflicts of interest

There are no conflicts to declare.

Acknowledgements

The authors are grateful to Project of Shanghai Municipal Science and Technology Commission (22DZ2291100), Sailing Project from the Science and Technology Commission of Shanghai Municipality (17YF1406600), Chenguang Project of Shanghai Municipal Education Commission and Shanghai Education Development Foundation (18CG68). X. W. thanks the support of Shanghai Polytechnic University for funding (EGD23QD03).

Notes and references

1 X. Wang, W. Cao, Z. Su, K. Zhao, B. Dai, G. Gao, J. Zhao, K. Zhao, Z. Wang, T. Sun, J. Han and J. Zhu, Fabrication of High Thermal Conductivity Nanodiamond/Aramid Nanofiber Composite Films with Superior Multifunctional Properties, *ACS Appl. Mater. Interfaces*, 2023, **15**(22), 27130–27143.

2 Z. Wei, P. Gong, X. Kong, M. Li, J. Cheng, H. Zhou, D. Li, Y. Ye, X. Lu, J. Yu and S. Lu, Enhanced Thermal Conductivity of Nanodiamond Nanosheets/Polymer Nanofiber Composite Films by Uniaxial and Coaxial Electrospinning: Implications for Thermal Management of Nanodevices, *ACS Appl. Nano Mater.*, 2023, **6**(10), 8358–8366.

3 L. Li, X. Yuan, H. Zhai, Y. Zhang, L. Ma, Q. Wei, Y. Xu and G. Wang, Flexible and Ultrathin Graphene/Aramid Nanofiber Carbonizing Films with Nacre-like Structures for Heat-Conducting Electromagnetic Wave Shielding/Absorption, *ACS Appl. Mater. Interfaces*, 2023, **15**(12), 15872–15883.

4 E. Jiao, K. Wu, Y. Liu, M. Lu, Z. Hu, B. Chen, J. Shi and M. Lu, Ultrarobust MXene-based laminated paper with excellent thermal conductivity and flame retardancy, *Composites, Part A*, 2021, **146**, 106417.

5 L. Si, Z. Lu, C. Yao, Q. Ma, Y. Zhao, Y. Wang, D. Wang and Z. Jin, Nacre-like nanocomposite film with excellent dielectric insulation properties and mechanical strength based on montmorillonite nanosheet and aramid nanofiber, *J. Mater. Sci.*, 2020, **55**(14), 5948–5960.

6 A. Patel, K. Wilcox, Z. Li, I. George, R. Juneja, C. Lollar, S. Lazar, J. Grunlan, W. E. Tenhaeff and J. L. Lutkenhaus, High Modulus, Thermally Stable, and Self-Extinguishing Aramid Nanofiber Separators, *ACS Appl. Mater. Interfaces*, 2020, **12**(23), 25756–25766.

7 K. Wu, J. Wang, D. Liu, C. Lei, D. Liu, W. Lei and Q. Fu, Highly Thermoconductive, Thermostable, and Super-Flexible Film by Engineering 1D Rigid Rod-Like Aramid Nanofiber/2D Boron Nitride Nanosheets, *Adv. Mater.*, 2020, **32**(8), 1906939.

8 G. Wang, D. Yu, A. D. Kelkar and L. Zhang, Electrospun nanofiber: emerging reinforcing filler in polymer matrix composite materials, *Prog. Polym. Sci.*, 2017, **75**, 73–107.

9 G. Xia, Q. Zhou, Z. Xu, J. Zhang, J. Zhang, J. Wang, J. You, Y. Wang and H. Nawaz, Transparent cellulose/aramid nanofibers films with improved mechanical and ultraviolet shielding performance from waste cotton textiles by *in situ* fabrication, *Carbohydr. Polym.*, 2021, **273**, 118569.

10 S. Gao, Y.-Z. Duan, Z.-N. Tian, Y.-L. Zhang, Q.-D. Chen, B.-R. Gao and H.-B. Sun, Laser-induced color centers in crystals, *Opt. Laser Technol.*, 2022, **146**, 107527.

11 A. N. Emin, How Composite Materials Influence Sustainable Development, *EuroEconomica*, 2021, **2**(40), 202–210.

12 C. Li, Y. Yang, G. Xu, Y. Zhou, M. Jia, S. Zhong, Y. Gao, C. Park, Q. Liu, Y. Wang, S. Akram, X. Zeng, Y. Li, F. Liang, B. Cui, J. Fang, L. Tang, Y. Zeng, X. Hu, J. Gao, G. Mazzanti, J. He, J. Wang, D. Fabiani, G. Teyssedre, Y. Cao, F. Wang and Y. Zi, Insulating materials for realising carbon neutrality: opportunities, remaining issues and challenges, *High Volt.*, 2022, **7**(4), 610–632.

13 B. Yao, H. Zhu, Y. Ding, C. Luo, T. Chen, J. Zhou, Y. Chen and P. Lin, Thermal management of electronics and thermoelectric power generation from waste heat enabled

by flexible Kevlar@SiC thermal conductive materials with liquid-crystalline orientation, *Energy Convers. Manage.*, 2022, **251**, 114957.

14 F. Su, J. Lin, Z. Huang, W. Xu and Y. Long, Thin superhydrophobic layers on the SiC powder surface toward electrical erosion resistance, *J. Mater. Sci.: Mater. Electron.*, 2023, **34**(5), 401.

15 L. W. Zeng, P. J. Xue and J. J. Bian, Si_3N_4 whisker/MPPO composite substrate with low dielectric loss and high thermal conductivity, *J. Mater. Sci.: Mater. Electron.*, 2022, **33**(21), 17190–17198.

16 R. Li, Z. Liu, R. Chen and S. Guo, *In situ* fabrication of polyimide microphase and its effects on the mechanical and dielectric properties of polytetrafluoroethylene composite films, *Composites, Part A*, 2023, **166**, 107381.

17 C. e. Yue, L. Guan, X. Zhang, Y. Wang and L. Weng, Thermally conductive epoxy/boron nitride composites with high glass transition temperatures for thermal interface materials, *Mater. Des.*, 2021, **212**, 110190.

18 X. Wang and P. Wu, Preparation of Highly Thermally Conductive Polymer Composite at Low Filler Content *via* a Self-Assembly Process between Polystyrene Microspheres and Boron Nitride Nanosheets, *ACS Appl. Mater. Interfaces*, 2017, **9**(23), 19934–19944.

19 A. Safeen, K. Safeen, R. Ullah, Zulfqar, W. H. Shah, Q. Zaman, K. Althubeiti, S. Al Otaibi, N. Rahman, S. Iqbal, A. Khan, A. Khan and R. Khan, Enhancing the physical properties and photocatalytic activity of TiO_2 nanoparticles *via* cobalt doping, *RSC Adv.*, 2022, **12**(25), 15767–15774.

20 R. Khan, M. I. Khan, M. K. Almesfer, A. Elkhaleefa, I. H. Ali, A. Ullah, N. Rahman, M. Sohail, A. A. Khan and A. Khan, The structural and dilute magnetic properties of (Co, Li) co-doped-ZnO semiconductor nanoparticles, *MRS Commun.*, 2022, **12**(2), 154–159.

21 R. Khan, I. Shigidi, S. Al Otaibi, K. Althubeiti, S. S. Abdullaev, N. Rahman, s. Mohammad, A. Khan, S. Iqbal, T. Del Rosso, Q. Zaman and A. Khan, Room temperature dilute magnetic semiconductor response in (Gd, Co) co-doped ZnO for efficient spintronics applications, *RSC Adv.*, 2022, **12**(55), 36126–36137.

22 R. Khan, V. Tirth, A. Ali, K. Irshad, N. Rahman, A. Algahtani, M. Sohail and S. Isalm, Effect of Sn-doping on the structural, optical, dielectric and magnetic properties of ZnO nanoparticles for spintronics applications, *J. Mater. Sci.: Mater. Electron.*, 2021, **32**(16), 21631–21642.

23 L.-C. Jia, Y.-F. Jin, J.-W. Ren, L.-H. Zhao, D.-X. Yan and Z.-M. Li, Highly thermally conductive liquid metal-based composites with superior thermostability for thermal management, *J. Mater. Chem. C*, 2021, **9**(8), 2904–2911.

24 S. Wang, X. Zhao, J. Luo, L. Zhuang and D. Zou, Liquid metal (LM) and its composites in thermal management, *Composites, Part A*, 2022, **163**, 107216.

25 S. K. Nayak, S. Mohanty and S. K. Nayak, Silver (Ag) nanoparticle-decorated expanded graphite (EG) epoxy composite: evaluating thermal and electrical properties, *J. Mater. Sci.: Mater. Electron.*, 2019, **30**(23), 20574–20587.

26 Zulfiqar, R. Khan, M. U. Rahman and Z. Iqbal, Variation of structural, dielectric and magnetic properties of PVP coated γ-Fe_2O_3 nanoparticles, *J. Mater. Sci.: Mater. Electron.*, 2016, **27**(12), 12490–12498.

27 L. Zhao, C. Liao, Y. Liu, X. Huang, W. Ning, Z. Wang, L. Jia and J. Ren, A combination of aramid nanofiber and silver nanoparticle decorated boron nitride for the preparation of a composite film with superior thermally conductive performance, *Compos. Interfaces*, 2022, **29**(4), 447–463.

28 D. Yang, Y. Ni, Y. Liang, B. Li, H. Ma and L. Zhang, Improved thermal conductivity and electromechanical properties of natural rubber by constructing Al_2O_3-PDA-Ag hybrid nanoparticles, *Compos. Sci. Technol.*, 2019, **180**, 86–93.

29 T. Huang, G. Zhang and Y.-h. Gao, A novel silver nanoparticle-deposited aluminum oxide hybrids for epoxy composites with enhanced thermal conductivity and energy density, *Compos. Interfaces*, 2019, **26**, 1001–1011.

30 J. Sun, Y. Yao, X. Zeng, G. Pan, J. Hu, Y. Huang, R. Sun, J.-B. Xu and C.-P. Wong, Preparation of Boron Nitride Nanosheet/Nanofibrillated Cellulose Nanocomposites with Ultrahigh Thermal Conductivity *via* Engineering Interfacial Thermal Resistance, *Adv. Mater. Interfaces*, 2017, **4**(17), 1700563.

31 K. Naito, Effect of Hybrid Surface Modifications on Tensile Properties of Polyacrylonitrile- and Pitch-Based Carbon Fibers, *J. Mater. Eng. Perform.*, 2016, **25**(5), 2074–2083.

32 Y. Lin, K. A. Watson, M. J. Fallbach, S. Ghose, J. G. Smith Jr, D. M. Delozier, W. Cao, R. E. Crooks and J. W. Connell, Rapid, Solventless, Bulk Preparation of Metal Nanoparticle-Decorated Carbon Nanotubes, *ACS Nano*, 2009, **3**(4), 871–884.

33 S. K. Nayak and D. Mohanty, Silver nanoparticles decorated α-alumina as a hybrid filler to fabricate epoxy-based thermal conductive hybrid composite for electronics packaging application, *J. Adhes. Sci. Technol.*, 2020, **34**(14), 1507–1525.

34 S. P. Pawar, S. Stephen, S. Bose and V. Mittal, Tailored electrical conductivity, electromagnetic shielding and thermal transport in polymeric blends with graphene sheets decorated with nickel nanoparticles, *Phys. Chem. Chem. Phys.*, 2015, **17**(22), 14922–14930.

35 R. Khan, K. Althubeiti, Zulfiqar, A. M. Afzal, N. Rahman, S. Fashu, W. Zhang, A. Khan and R. Zheng, Structure and magnetic properties of (Co, Ce) co-doped ZnO-based diluted magnetic semiconductor nanoparticles, *J. Mater. Sci.: Mater. Electron.*, 2021, **32**(19), 24394–24400.

36 M. u. Rahman, M. Saqib, K. Althubeiti, K. M. Abualnaja, S. u. Zaman, N. Rahman and R. Khan, Effect of Sr and Co co-doping on the TiO_2-diluted magnetic semiconductor for spintronic applications, *J. Mater. Sci.: Mater. Electron.*, 2021, **32**(24), 28718–28729.

37 R. Khan, S. Al Otaibi, A. J. Babqi, N. Rahman, M. sohail, R. M. Yusupov, S. S. Abdullaev, A. Khan, S. Iqbal, T. Del Rosso, Tahir, Q. Zaman and A. Khan, Structural, dielectric, and magnetic responses in doped ZnO magnetic nanoparticles for spintronics, *J. Mater. Sci.: Mater. Electron.*, 2023, **34**(3), 169.

38 M. Hussain, R. Khan, Zulfiqar, T. Z. Khan, G. Khan, S. Khattak, M. U. Rahman, S. Ali, Z. Iqbal, Burhanullah and K. Safeen, Dielectric and magnetic properties of cobalt doped γ-Fe_2O_3 nanoparticles, *J. Mater. Sci.: Mater. Electron.*, 2019, **30**(14), 13698–13707.

39 S. Li, J. Li, N. Ma, D. Liu and G. Sui, Super-Compression-Resistant Multiwalled Carbon Nanotube/Nickel-Coated Carbonized Loofah Fiber/Polyether Ether Ketone Composite with Excellent Electromagnetic Shielding Performance, *ACS Sustainable Chem. Eng.*, 2019, 7(16), 13970–13980.

40 Z. Cai, L. Su, H. Wang, Q. Xie, H. Gao, M. Niu and D. Lu, Hierarchically assembled carbon microtube@SiC nanowire/Ni nanoparticle aerogel for highly efficient electromagnetic wave absorption and multifunction, *Carbon*, 2022, **191**, 227–235.

41 B. Yang, L. Wang, M. Zhang, J. Luo and X. Ding, Timesaving, High-Efficiency Approaches To Fabricate Aramid Nanofibers, *ACS Nano*, 2019, **13**(7), 7886–7897.

42 C. V. Restrepo and C. C. Villa, Synthesis of silver nanoparticles, influence of capping agents, and dependence on size and shape: a review, *Environ. Nanotechnol., Monit. Manage.*, 2021, **15**, 100428.

43 M. Lin, Y. Li, K. Xu, Y. Ou, L. Su, X. Feng, J. Li, H. Qi and D. Liu, Thermally conductive nanostructured, aramid dielectric composite films with boron nitride nanosheets, *Compos. Sci. Technol.*, 2019, **175**, 85–91.